

Near-infrared photometry and spectroscopy of the low Galactic latitude globular cluster 2MASS-GC 03

Julio A. Carballo-Bello^{1,2,8} ^{*}, S. Ramírez Alegría^{1,2}, J. Borissova^{1,2}, L. C. Smith³, R. Kurtev^{1,2}, P. W. Lucas³, Ch. Moni Bidin⁴, J. Alonso-García^{5,2}, D. Minniti^{6,2,7}, T. Palma^{2,6}, I. Dékány^{8,2}, N. Medina^{2,1}, M. Moyano⁴, V. Villanueva^{2,1} and M. A. Kuhn^{1,2}

¹*Instituto de Física y Astronomía, Facultad de Ciencias, Universidad de Valparaíso, Av. Gran Bretaña 1111, Playa Ancha, Casilla 5030, Valparaíso, Chile*

²*Millennium Institute of Astrophysics, Av. Vicuña Mackenna 4860, 7820436, Macul, Santiago, Chile*

³*Centre for Astrophysics Research, Science and Technology Research Institute, University of Hertfordshire, Hatfield AL10 9AB, UK*

⁴*Instituto de Astronomía, Universidad Católica del Norte, Av. Angamos 0610, Antofagasta, Chile*

⁵*Unidad de Astronomía, Facultad de Cs. Básicas, Universidad de Antofagasta, Av. U. de Antofagasta 02800, Antofagasta, Chile*

⁶*Departamento de Física, Facultad de Ciencias Exactas, Universidad Andrés Bello, Av. Fernández Concha 700, Las Condes, Santiago, Chile*

⁷*Vatican Observatory, V00120 Vatican City State, Italy*

⁸*Instituto de Astrofísica, Facultad de Física, Pontificia Universidad Católica de Chile (IA-PUC), Casilla 306, Santiago 22*

Accepted ??

ABSTRACT

We present deep near-infrared photometry and spectroscopy of the globular cluster 2MASS-GC 03 projected in the Galactic disk using MMIRS on the Clay telescope (Las Campanas Observatory) and VISTA Variables in the Via Lactea survey (VVV) data. Most probable cluster member candidates were identified from near-infrared photometry. Out of ten candidates that were followed-up spectroscopically, five have properties of cluster members, from which we calculate $\langle[\text{Fe}/\text{H}]\rangle = -0.9 \pm 0.2$ and a radial velocity of $\langle v_r \rangle = -78 \pm 12$ km/s. A distance of 10.8 kpc is estimated from 3 likely RR Lyrae members. Given that the cluster is currently at a distance of 4.2 kpc from the Galactic center, the cluster’s long survival time of an estimated 11.3 ± 1.2 Gyr strengthens the case for its globular-cluster nature. The cluster has a hint of elongation in the direction of the Galactic center.

Key words: keywords

1 INTRODUCTION

Galactic globular clusters (GCs) have played a role in diverse areas of study, from the evolution of stellar populations to the hierarchical formation of galaxies. The current population of known GCs in the Milky Way is composed of ~ 160 of these systems (Harris, 2010), although it has long been suggested (e.g. Ashman & Zepf, 1992) that a fraction of the total number of Galactic GCs might be hidden in lines of sight with high extinction (i.e. disk, bulge) or have intrinsic properties that make them difficult to detect. The search for new Galactic GCs has only returned a small number of the expected missing GCs. Some of these newly identified GCs have properties mid-way between a GC and an ultra-faint dwarf galaxy (Carraro, 2005, Willman et al., 2005, Koposov et al., 2007, Longmore et al., 2011, Muñoz et al., 2012, Balbinot et al., 2013, Laevens et al., 2014, Kim et al., 2015).

Most of these new detections were possible thanks to the arrival of wide-sky photometric surveys such as Sloan Digital Sky Survey (SDSS, York et al., 2000), the Two Micron All Sky Survey (2MASS, Skrutskie et al., 2006) and the VISTA Variables in the Via Lactea (VVV) Public Survey (Minniti et al., 2010, Saito et al., 2012). The latter survey reported the discovery of VVV CL 001 (Minniti et al., 2011), VVV CL 002 (Moni Bidin et al., 2011) and several other GC candidates (Borissova et al., 2014).

It is well known that the Galactic GC system contains a metal-rich subsystem (Zinn, 1985) which is mainly composed of GCs associated with the Galactic bulge. Among the 13 GCs found with $|b| < 2^\circ$ (8% of the Galactic population), 11 lie projected on the Galactic bulge, while only two, 2MASS-GC 03 and GLIMPSE 01 (Simpson & Cotera, 2004, Kobulnicky et al., 2005, Davies et al., 2011), are likely associated with the Milky Way disk. However, the nature of GLIMPSE 01 remains unclear (see Davies et al., 2011). In contrast, numerous young cluster candidates have been

* E-mail: julio.carballo@uv.cl

discovered in the Galactic plane using infrared photometry (e.g. Froebrich et al., 2007, Borissova et al., 2011; 2014, Solin et al., 2014). Therefore, the scarce GCs at low Galactic latitudes represent a peculiar population of stellar systems in a region of the Milky Way dominated by the presence of young stellar clusters.

Froebrich et al. (2007) first identified 2MASS-GC 03 as a local density enhancement in 2MASS photometry maps, listing it as #1735 (or FSR 1735) in their catalog. Follow-up JHK_s photometry of stars associated with that overdensity (Froebrich et al., 2007) allowed the authors to suggest that FSR 1735 is actually a GC at $d_{\odot} \sim 9$ kpc, although they point out that a definitive determination of the object's nature would require follow-up observations. A systematic analysis of the cluster was performed by Kharchenko et al. (2013), as a part of a global investigation on the Galactic star-cluster system. Using the 2MASS catalogs and PPMXL Catalogue of Positions and Proper Motions on the ICRS (Roeser et al., 2010), they estimated the metallicity, distance and age of FSR 1735 as $[\text{Fe}/\text{H}] = -0.6$, $d_{\odot} \sim 8.8$ kpc and $t = 9.9$ Gyr, respectively. Because of its discovery in 2MASS data, FSR 1735 has the SIMBAD denomination 2MASS-GC03 and it also corresponds to the candidate number 71 in the Solin et al. (2014) catalog, which contains new star cluster candidates discovered in the VVV field of view. In this paper, we will use the SIMBAD designation, namely 2MASS-GC03 or simply GC03. As it can be seen in Figure 1, we observe a clear overdensity of stars in the VVV K_s -image, but it is not associated with mid-infrared nebulosity in WISE images (Figure 1, right panel), confirming the Froebrich et al. conclusion of small amounts of dust and gas in that area.

In this paper, we present deep MMIRS and VVV photometry and low-resolution near-infrared spectroscopy of several stars in order to confirm the globular nature of the cluster GC03 and derive accurate values for the fundamental parameters that describe that system.

2 OBSERVATIONS AND DATA REDUCTION

The analysis of GC 03 (RA= $16^{\text{h}}52^{\text{m}}10.6^{\text{s}}$, DEC= $-47^{\circ}03'29''$ Harris, 2010) includes near-infrared images and spectra, both obtained using the MMT and Magellan Infrared Spectrograph (MMIRS, McLeod et al., 2012) at the Clay Telescope (Las Campanas Observatory, Chile). The instrument is a wide field near-infrared imager and spectrograph. We have complemented our data using the VVV JHK_s photometry.

With the MMIRS, the cluster was observed through J and K_s filters, with a total exposure time per filter of 119 seconds and airmasses between 2.35 and 2.08. We used a dithering pattern with offsets in x and y-axis of 34 arcsec; these offsets in the images are used later to construct the calibration image for sky subtraction. We reduced the imaging data using IRAF¹ tasks (dark subtraction, flat fielding,

and sky correction) and we used python package ALIPY² to align the individual reduced images before the final combination.

The PSF photometry was independently derived for each of the images using DAOPHOT II/ALLSTAR (Stetson, 1987). The calibration of the photometric catalogs was performed using the ~ 1000 stars in common with 2MASS, and we substitute 2MASS photometry for objects that are saturated or present other problems in the PSF photometry procedure. The magnitudes obtained from individual images were averaged for the final catalog. To estimate completeness, artificial stars were inserted randomly throughout the chip in the range $10 < K_s < 20$ mag, and these were extracted using the same photometric procedure. The total number of synthetic stars added was designed not to exceed 15% of the number of natural sources. This procedure was performed 50 times for each frame. The average magnitude limits of our catalogs, where the fraction of synthetic stars recovered is the 50%, are 18.6 mag and 17.6 mag in J and K_s , respectively.

To select promising candidates for spectroscopy, we used PSF photometry from the VVV-SkZ pipeline (Mauro et al., 2013), an automated software based on ALLFRAME (Stetson, 1987) and optimized for VISTA PSF photometry. We used J and K_s images from the VVV survey (Minniti et al., 2010) and replaced the photometry from saturated sources (i.e. brighter than $K_s = 12$), with 2MASS photometry. Position and near-infrared colors and magnitudes were used to remove likely contaminants from the photometric catalog using the algorithm of Bonatto & Bica (2010), as described by Borissova et al. (2011). The preliminary decontaminated CMDs allowed us to select bright ($6.56 < K_s < 11.82$) cluster member candidates for multi-object spectroscopy. We selected 10 stars to observe with a single mask with MMIRS, using the HK grism, a slit width of 0.4 arcsec, and a resolution $R \sim 1400$.

Standard IRAF procedures were used to de-bias and flat-field the spectra. The 10 one-dimensional spectra were extracted, and the wavelength calibration was obtained using a third-order polynomial fit to ~ 40 arc lines, resulting in a dispersion of $\sim 6.7\text{\AA} \text{ pix}^{-1}$ and a rms scatter of 0.4\AA . We corrected the atmospheric absorption lines with MOLECFIT (Kausch et al., 2015, Smette et al., 2015), a software tool distributed by ESO which uses the information available in the spectra header to model the atmospheric and telescope conditions and the telluric lines during the observations. The resulting spectra are shown in Figure 2.

3 RESULTS

The cluster center was determined with an iterative procedure based on a VVV photometric catalog of stars brighter than $K_s = 17$. We first calculated the barycenter of all the sources detected within 1 arcmin from the Froebrich et al. (2007) coordinates. The point thus found was adopted as new cluster center, and the calculation iterated. The procedure quickly converged to fluctuations smaller than one pixel ($0''.33$) around the values RA= $16^{\text{h}}52^{\text{m}}11.1^{\text{s}}$,

¹ IRAF is distributed by the National Optical Astronomy Observatories (NOAO), which is operated by the Association of Universities for Research in Astronomy, Inc. (AURA) under cooperative agreement with the U.S.A. National Science Foundation (NSF).

² <http://obswww.unige.ch/~tewes/alipy/>

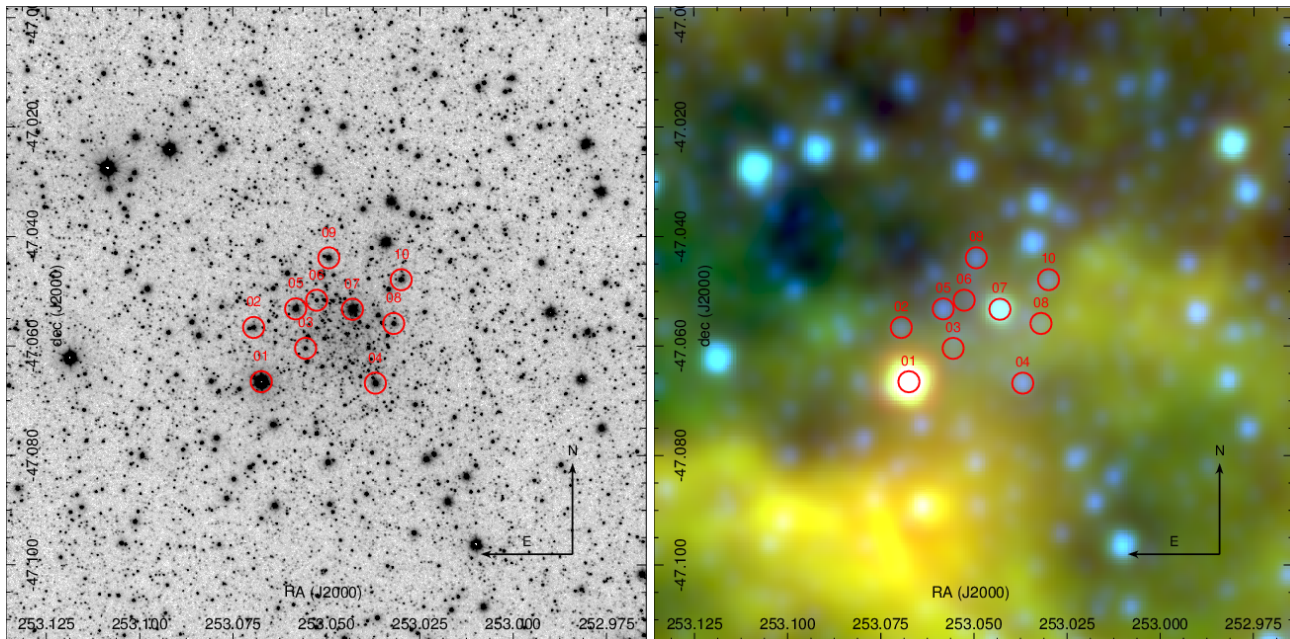


Figure 1. VVV K_S (left) and WISE false color (right) images for GC03. The red circles show the position of the stars observed spectroscopically. The false color image was constructed using the WISE filters W1 (blue), W2 (green) and W3 (red). The image sizes are 7 arcmin \times 7 arcmin.

DEC= $-47^{\circ}3'30''$, which represents our best estimate of the cluster center. This is only $7''.6$ offset from Froebrich et al. (2007) coordinates.

3.1 Decontaminated color-magnitude diagram

To determine the most probable cluster members we used the deeper MMIRS photometry. As expected for low Galactic latitudes and poorly populated targets, the near-infrared point-source catalogs were dominated by field stars. Therefore statistical decontamination of the photometric catalog is necessary to provide a cleaner sample of the GC 03 stellar population that will be used for further analysis. The algorithm we use (proposed by Bonatto & Bica (2007)), is based on a multivariate search for over-densities in the JHK_s catalogs. Although the cluster membership cannot be determined absolutely, the algorithm is rather effective at removing the majority of field stars. As described in more detail in Bonatto & Bica (2007) paper, the algorithm divides the $(K_s, J - K_s)$ color-magnitude space into a grid of cells with a cell size provided as input. It estimates the expected number density of cluster stars for each of the cells by subtracting the field stars number density in the same $(K_s, J - K_s)$ ranges and, summing over all cells, it obtains a total number of candidate stars N_{mem} . The procedure is repeated with the grid shifted in steps of $1/3$ cell width in each dimension, yielding 9 different configurations, with nine different N_{mem} values. Those stars that *survive* to this process more than $\langle N_{\text{mem}} \rangle$ times are considered likely members. For this work, we slightly modified the procedure by including a family of cell sizes both for K_s and $J - K_s$ in the range $0.2 < \delta K_s < 0.6$ and $0.1 < \delta(J - K_s) < 0.3$. We generated a list of tentative cluster members derived from 15 iterations, based on the number of times that a star was present in the

results. As a final step, we ranked the stars depending on that survival frequency and assigned a probability, P_{memb} , to each star based on their frequency of survival. Thus, it is possible to select stars using a different P_{memb} threshold for more or less reliable subsamples. The procedure was applied within a radius of 1.5 arcmin of the cluster center, which contains, from visual analysis, the greatest density of stars.

Figure 3 shows the importance of the decontamination process to obtain useful CMDs. From the initial 1649 sources within 1.5 arcmin from the center of GC 03 (middle panel), our algorithm found 348 candidate stars for any P_{mem} value. Focusing on those stars with the highest membership probabilities, $P_{\text{mem}} > 0.5$, the sample of member stars is reduced to 315 sources.

As shown in Figure 3, the decontaminated CMD shows a well defined Red-Giant Branch (RGB) in the range $12 < K_s < 16.5$ mag. A conspicuous overdensity is found at $K_s \sim 14.4$ mag that could be composed of Red Horizontal Branch stars (HB). However, the detection of Milky Way Red Clump (RC) stars in our field is also expected given that they are the dominant population among the Galactic giant stars. In fact, they have been long used to trace the Galactic structure because of their narrow luminosity function (e.g. Cabrera-Lavers et al., 2008, McWilliam & Zoccali, 2010, González-Fernández et al., 2014). To confirm the association of that overdensity of stars with the cluster, we constructed area-normalized luminosity functions by counting stars in the range $1 < J - K_s < 1.5$ and $12 < K_s < 18$ with a bin size of $\delta K_s = 0.2$ for all the sources within 1.5 arcmin from the cluster center and for those stars beyond 1.5 arcmin. The results (see Figure 4) show a discrepancy between the distributions for the field and cluster areas and a peak is found at $K_s \sim 14.4$ mag. The lack of a significant component of field stars in that position confirms that only

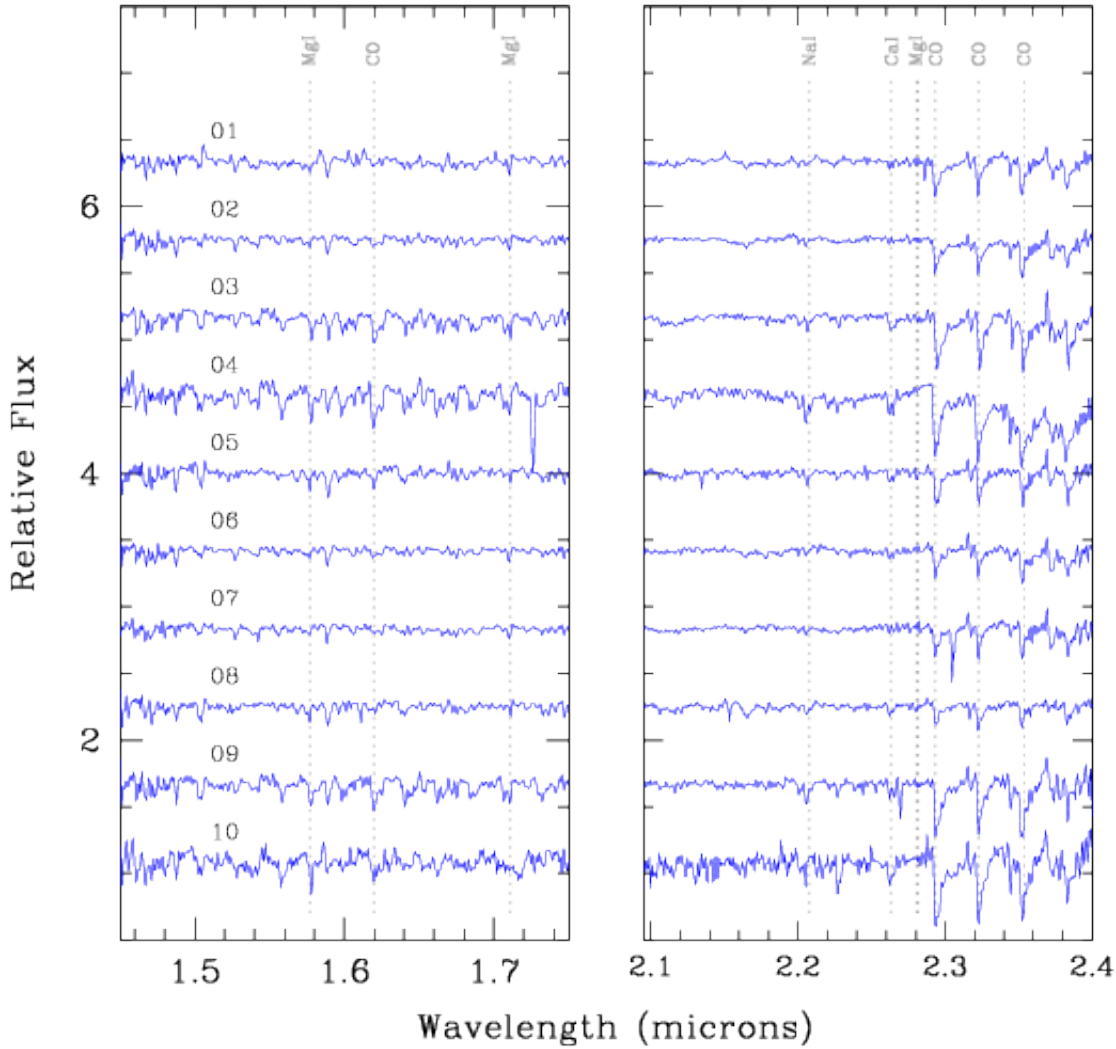


Figure 2. Individual spectra in H (left) and K band (right) for the observed stars. We marked with grey vertical lines the spectral lines used for metallicity and radial velocity estimates.

a stellar population in the $r < 1.5$ arcmin region, lying in an extremely narrow distance range, is able to generate such a well-defined feature in the CMD. Thus, we conclude that the overdensity detected in $K_s \sim 14.4 \pm 0.2$ mag corresponds to the RHB of GC 03, also detected by Froebrich et al., but 0.4 mag fainter in K_s . The distributions shown in Figure 4 suggests an additional second peak at $K_s \sim 15.1$. This was suggested by Froebrich et al. (2007), although they reported that its presence depended on the magnitude bin used to construct the luminosity function. The profile of the peak varies slightly with different bin sizes but the double peak morphology is always observed. As for the RC, the absence of a significant variation of stellar counts in the field around GC 03, suggests that this hypothetical second overdensity is associated with the cluster. We propose that these stars

are crossing the so-called Red Giant Branch Bump (RGBB), a transitory variation in the magnitude of RGB stars produced by a discontinuity in the chemical abundance profile, which is detected in a significant number of Galactic GCs (e.g. Valenti et al., 2007, Nataf et al., 2013, and references therein). However, the additional investigation of RGBBs is beyond the scope of our work with the data available. The peak around $K_s = 12.6$ mag, which appear in the Froebrich et al. CMD and was interpreted as AGB bump, is not found.

3.2 Metallicity and radial velocity

To calculate the $[\text{Fe}/\text{H}]$ values of the spectroscopically measured stars, we used the metallicity calibration by Frogel et al. (2001), based on the Equivalent Width (EW) of the

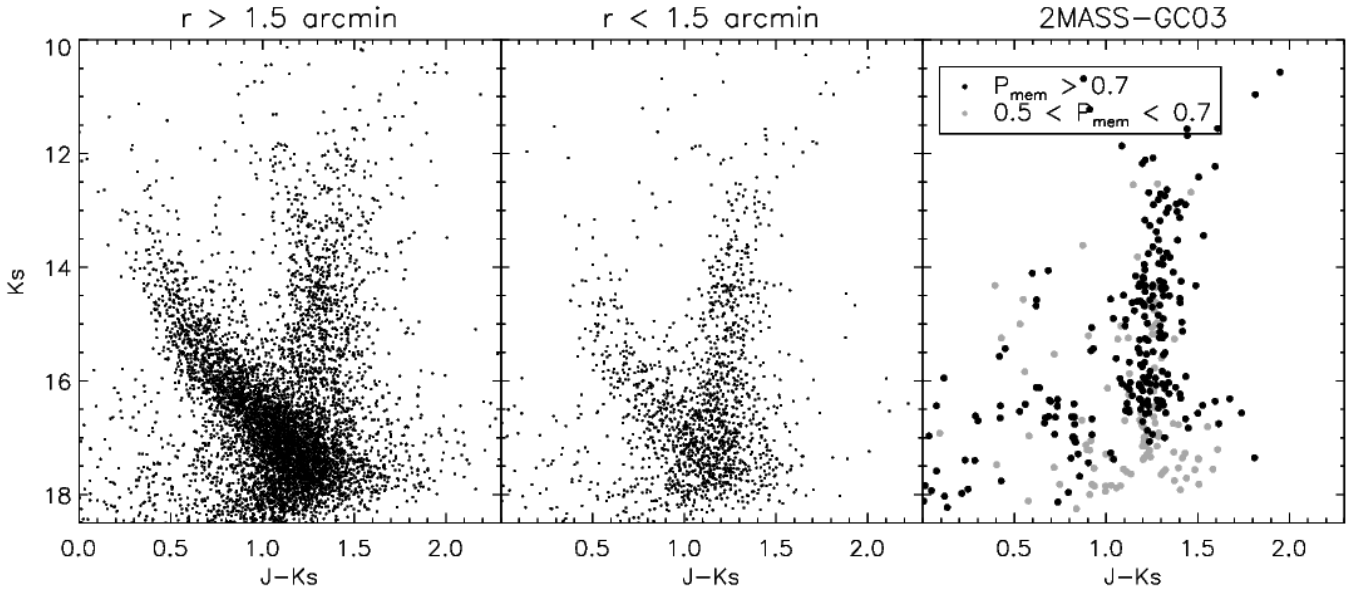


Figure 3. CMDs corresponding to stars beyond and within 1.5 arcmin of the cluster center (left and middle panels respectively) and the resulting decontaminated CMD (right panel). The latter panel displays stars with higher probability of membership ($P_{\text{mem}} > 0.7$) as black dots while stars with lower membership probability ($0.5 > P_{\text{mem}} > 0.7$) are shown in grey.

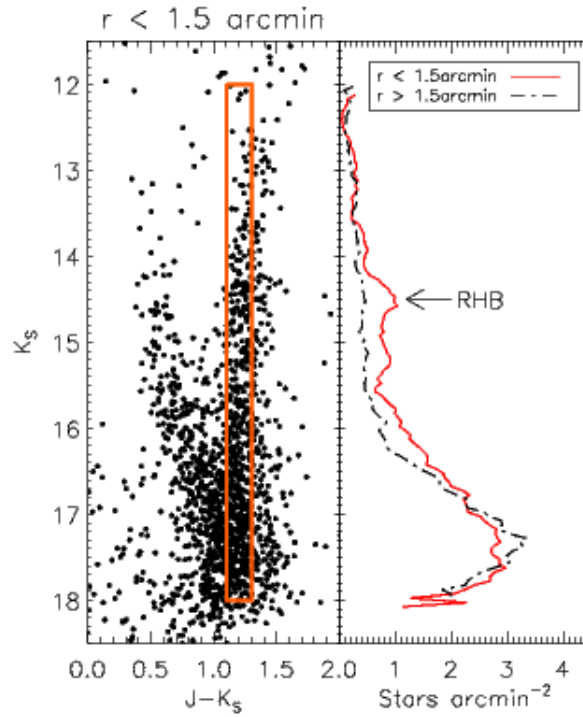


Figure 4. *Left:* CMD corresponding to all stars contained in the area with $r < 1.5$ arcmin from the center of GC 03. The overplotted orange box indicates the region of the CMD used to derive the luminosity functions. *Right:* luminosity function for all stars with $r < 1.5$ arcmin (red) and field stars beyond 1.5 arcmin from the cluster center (dotted black line). The position of RHB is indicated with an arrow.

NaI 2.21 μm and CaI 2.26 μm lines and the ^{12}CO (2,0) band. The calibration is particularly useful for moderate-resolution K -band spectra and was completed using spectra from 15 GCs. We measured the EW of our targets on the continuum normalised spectra, with the IRAF task *splot*. In general, we fit line profiles using a Gaussian with a linear background, and in more complicated profiles we used the deblending function or Voigt profile fitting. The EW uncertainties were estimated taking into account the S/N of the spectra, the peak to continuum ratio of the line and the error from the telluric star subtraction (which was estimated to be $\sim 10\%$ in the worst cases). The uncertainties of the Frogel et al. (2001) calibration are assumed to be 0.2 dex.

We measured the radial velocities (RVs) of the targets with the IRAF task *rvidlines*, which fits spectral lines to determine the wavelength shift with respect to specified rest wavelengths. In this procedure, we used the Mg I (at 1.5770, 1.7109 and 2.2813 μm), NaI (at 2.2062 and 2.2090 μm), CaI (at 2.2631 and 2.2657 μm) lines and the ^{12}CO (6,3), (2,0) and (3,1) bands, available in the spectra (typically 7–10 lines per spectrum). To calculate uncertainties, we added in quadrature the line-measurements errors from *rvidlines* and the errors from the wavelength calibration of each spectrum. Table 1 gives the metallicity and radial velocities for the stars with spectroscopic follow-up.

3.3 Proper motions of GC 03

At the distance of the cluster given by Froebrich et al. (2007), $d_{\odot} = 9.1\text{ kpc}$, the five-year VVV baseline is not enough to provide a precise separation of the cluster members and the field stars by proper motion analysis. Nevertheless, using a proper motion pipeline developed by Smith (2015), we were able to estimate the mean relative motion of the cluster. Briefly, the proper motion pipeline splits each array of the VVV catalog at every epoch into 5×5 sub-arrays. The coordinate system of each sub-array at each epoch is transformed to the master epoch (the epoch with best seeing) coordinate system using a linear fit and an iterative rejection of astrometric reference sources with significant ($> 3\sigma$) residuals. The proper motions are fit in array coordinate space using the Levenberg-Marquardt algorithm through the CURVE_FIT function of the SCIPY.OPTIMIZE package. Individual epochs are iteratively removed if they are ($> 3\sigma$) from the fit. The final array coordinate motions are converted to equatorial coordinates using the astrometric fit parameters of the master epoch, which are produced by CASU and contained in the FITS header information. The mean uncertainty of the method up to $K_s = 14\text{ mag}$ is under 1 mas/yr on average. Thus, we have selected only stars with $K_s < 14\text{ mag}$ and radius 0.9 arcmin from the cluster center determined in the previous paragraph (red points in Figure 5, left) and compare them with the sources within 5 arcmin in the same magnitude interval (grey points) on the $\mu_{\alpha \cos \delta}$ vs. μ_{δ} proper motion diagram. As can be seen, the cluster members are mostly concentrated in a clump in this proper motion diagram, while field stars are much more spread out. The values resulting from the Gaussian fits of the proper motion distributions are $\mu_{\alpha \cos \delta} = -1.3 \pm 0.2$ and $\mu_{\delta} = +1.8 \pm 0.3$ for the mean relative proper motion of the cluster (expressed in mas/yr; the errors correspond to the fitting errors). By taking all stars within a $\pm 1\text{ mas/yr}$ box

centered on the proper motion clump and highlighting them in a $J - K_s$ vs. K_s color magnitude (Figure 5, right), we show that the method predominantly select the giants that are cluster members and excluded field dwarfs.

3.4 Memberships of the spectroscopic targets

The spectroscopic targets were selected from statistically decontaminated photometry (see Sect. 2). However, our statistical decontamination methods are not designed to definitively determine cluster membership. As a result, we inevitably obtained some spectra of field stars. Cluster membership could be determined more accurately from the proper motion, radial velocity and metallicity histograms. The left panel of Figure 6 shows the distance of the star from the cluster center, metallicity and relative proper motion vs. measured radial velocities of the spectroscopically observed stars. It was not possible to use the relative proper motion of spectroscopically observed stars to separate field stars from cluster members, because only six of them have measured proper motions, the rest are saturated in the VVV images. In addition, using the Bonatto & Bica (2011) algorithm, we fitted the radial velocity and $[\text{Fe}/\text{H}]$ distributions with a Gaussian profile. The resulting values of the Gaussian fits are as $[\text{Fe}/\text{H}] = -0.98 \pm 0.05$ (dex), $\mu = 1.4 \pm 0.4\text{ mas/yr}$ and $\text{RV} = -69 \pm 3\text{ km/s}$.

The analysis of such constructed diagrams shows that stars number 3, 4, 5, 9 and 10 are definitely outliers from the fitted distributions and thus are considered field stars. The stars number 1, 2, 6, 7 and 8 are probable cluster members. Looking at the position of the stars numbers 1 and 7 on the CMD (Figure 6, right panel) we can speculate that most probably these stars are red variables, but they are saturated in VVV images so it is not possible to test this suggestion.

Considering only cluster member stars (number 1, 2, 6, 7 and 8), the mean metallicity and radial velocity for GC 03 are calculated as $\langle [\text{Fe}/\text{H}] \rangle = -0.9 \pm 0.2$ and $\langle v_r \rangle = -78 \pm 12\text{ km/s}$. Such calculated $[\text{Fe}/\text{H}]$ value is in agreement with the metallicity interval reported in Froebrich et al. (2007) and lower than Kharchenko et al. (2013) estimate. However, we have to point out that this is a first spectroscopic determination, while the above cited authors used photometric calibrations to derive the metallicity.

3.5 Variable stars

Using the VVV five year database we searched for variability within 15 arcmin radius from the cluster center. Forty nine K_s epochs are available between 2010 and 2014, the searching method was focused on variations in the light curves greater than 0.2 in K_s (conservative upper limit of our photometry, including the photometric errors, calibration to the standard system, etc.). Three variables are found, namely V1, V2 and V3, with mean K_s magnitudes $\langle K_s \rangle = 14.83, 15.22$ and 15.38 mag , respectively. Using the information potential metric developed in Huijse et al. (2011) we found their periods in the range $0.48 < P < 0.55\text{ days}$. Thus, they are classified as RRab Lyrae stars. Their coordinates are listed in Table 7 and their position in the CMD is shown in Figure 6. Note, that we plotted the mean K_s magnitude and random phase of corresponding J ones. The light curves are shown in Figure 7.

ID	RA [J2000]	DEC [J2000]	K_s	$J - K_s$	[Fe/H]	RV [km s ⁻¹]	$\mu_{\alpha \cos \delta}$ [mas y ⁻¹]	μ_{δ} [mas y ⁻¹]
01*	16:52:16.2	-47:03:59.5	6.56 ± 0.03	2.40 ± 0.04	-0.95 ± 0.18	-95 ± 11	---	---
02*	16:52:16.7	-47:03:23.9	10.32 ± 0.04	2.14 ± 0.06	-0.93 ± 0.20	-83 ± 12	$+0.06 \pm 0.88$	-2.35 ± 0.89
03	16:52:13.4	-47:03:37.6	11.34 ± 0.03	1.18 ± 0.04	-0.18 ± 0.33	$+112 \pm 14$	$+5.01 \pm 0.57$	$+0.95 \pm 0.58$
04	16:52:08.9	-47:04:00.5	9.54 ± 0.02	1.9 ± 0.2	$+0.74 \pm 0.49$	-60 ± 10	---	---
05	16:52:14.0	-47:03:11.7	9.60 ± 0.03	1.98 ± 0.04	-0.57 ± 0.26	0 ± 9	---	---
06*	16:52:12.6	-47:03:06.0	11.84 ± 0.07	2.53 ± 0.05	-0.76 ± 0.22	-75 ± 10	$+1.42 \pm 0.58$	-1.60 ± 0.59
07*	16:52:10.3	-47:03:11.9	8.21 ± 0.04	2.53 ± 0.05	-0.97 ± 0.20	-72 ± 9	---	---
08*	16:52:07.7	-47:03:21.2	10.63 ± 0.03	2.31 ± 0.04	-0.82 ± 0.22	-63 ± 11	-1.95 ± 0.61	-4.33 ± 0.60
09	16:52:11.8	-47:02:38.1	9.85 ± 0.03	2.02 ± 0.04	-0.04 ± 0.34	0 ± 12	$+13.77 \pm 1.75$	$+17.24 \pm 1.75$
10	16:52:07.2	-47:02:52.5	9.99 ± 0.02	1.98 ± 0.03	$+0.22 \pm 0.40$	$+14 \pm 20$	-1.35 ± 0.99	$+4.79 \pm 1.01$

Table 1. K_s , $K_s - J$, metallicity, radial velocity and relative proper motions derived for the stars with spectroscopic follow-up. Asterisks indicate likely cluster members. The proper motions are relative.

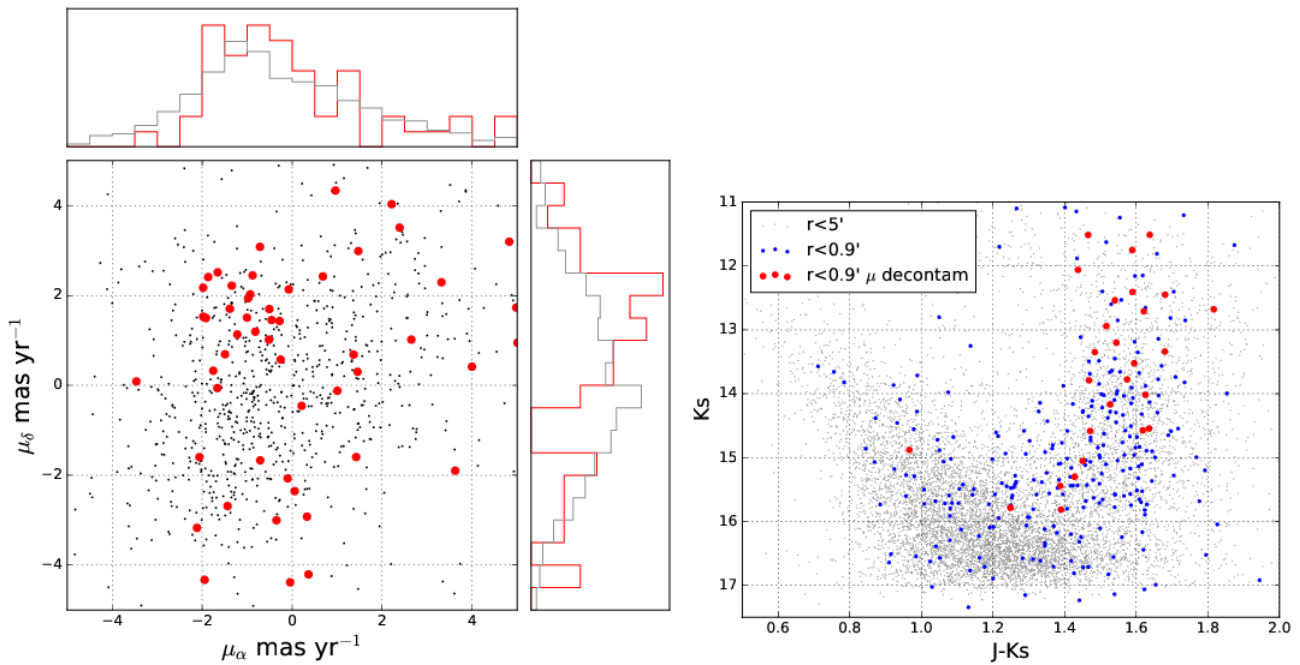


Figure 5. Left panel: Pipeline proper motions of $K_s < 14$ mag sources within 5 arcmin (grey points), and 0.9 arcmin (red points) of the globular cluster GC03. Notice the concentration of red points in PM space. Right: The $J - K_s$ vs. K_s color magnitude diagram, the grey points are stars with $K_s < 14$ mag within 5 arcmin, the blue points are stars within 0.9 arcmin from the cluster center, the red points stand for the star with similar (± 1 mas/yr).

Assuming that these RR Lyrae stars are associated with GC03, the period–luminosity calibration from Muraveva et al. (2015) gives a mean heliocentric distance to the cluster of $d_{\odot} = 10.8 \pm 0.4$ kpc. The RR Lyrae calculated distance value is bigger than previously found by Froebrich et al. and Kharchenko et al. 2013 and we will adopt $d_{\odot} = 10.8 \pm 0.9$ kpc, as our final distance determination, adding quadratically the conservative limit of the errors from photometry, calibration, etc.

3.6 Isochrone fitting

To constrain the age, we generated a grid of the theoretical isochrones from Padova library (Bressan et al., 2012) with ages between 6–12 Gyr with metallicity fixed on the value

derived above. We also fixed the distance to the above calculated from RR Lyrae stars value. Then, we fitted these isochrones to the observed CMD and reasonable matches were obtained within range of ages. Given that our photometry does not reach the turn-off level of the population, the isochrones with ages in the range 10–12.5 Gyr are suitable to reproduce the observed CMD, which is consistent with the presence of RR Lyrae stars. Therefore, we adopt a mean value of $t = 11.3 \pm 1.2$ Gyr with a distance modulus of $(m - M)_0 = 15.17 \pm 0.5$ and $A_K = 0.37$. The isochrones are overplotted in Figure 6 and the parameters derived are shown in Table 2.

Based in our heliocentric distance, we estimate that the distance with respect to the plane for GC 03 is $|z| \sim 350$ pc. Given that the scale heights for the thin and thick disks are

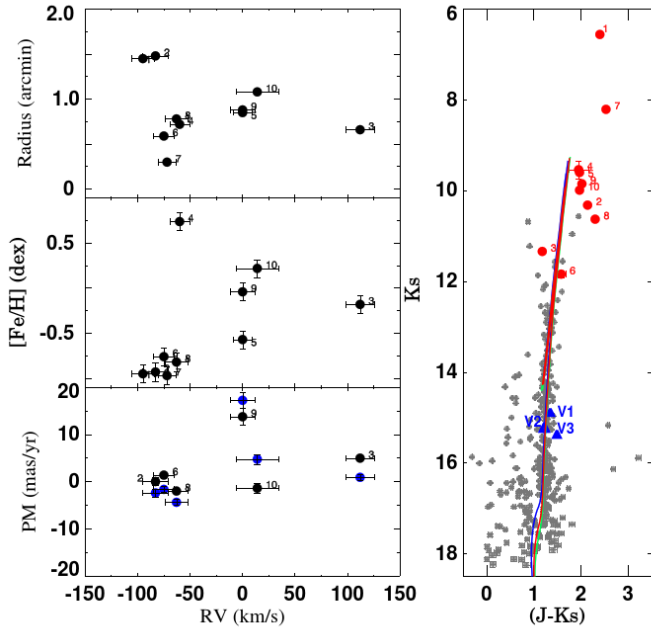


Figure 6. Left: Distance of the spectroscopic target stars with respect to the cluster center in arcmin, the measured $[\text{Fe}/\text{H}]$ in dex, the relative proper motion $\mu_{\alpha \cos \delta}$ (black) and μ_{δ} (blue) in mas/year as a function of the RV in km/s. The error bars represent the random errors of the measurements. Right: The $(J - K_s)$ vs. K_s CMD of the statistically decontaminated most probable cluster members. The spectroscopically observed stars are plotted as red circles while RR Lyrae stars are plotted as blue triangles. The error bars represent the photometric errors and the isochrones with ages $t = 9.8, 10$ and 12.6 Gyr are overlotted as a blue, red and green solid lines, respectively.

set, respectively, in $h_z = 300$ and 900 pc (Jurić et al., 2008), we confirm that this cluster is immersed in the Galactic disk. Its location in the Galaxy together with the parameters derived above might help us establish the nature of GC 03. While young stellar clusters ($t < 500$ Myr) are concentrated towards the plane, older open clusters (OCs) show an exponential distribution with scale heights greater than 375 pc and as a function of age (Janes & Phelps, 1994, Joshi, 2005, Bonatto et al., 2006, Buckner & Froebrich, 2014). In this context, GC 03 might belong to the Galactic OC population becoming one of its oldest members known, ~ 2 Gyr older than NGC 6791 (Brogaard et al., 2012) and with a similar age to that of Berkeley 17 (Krusberg & Chaboyer, 2006). On the other hand, the mean $[\text{Fe}/\text{H}]$ derived for old ($t > 1$ Gyr) OCs in the Galaxy contained in the WEBDA³ compilation is $[\text{Fe}/\text{H}] = -0.2 \pm 0.3$, where the old Berkeley 17 presents a metallicity of $[\text{Fe}/\text{H}] = -0.3$. GC 03 is thus metal-poorer than the bulk of OCs, including coeval clusters.

The radial distribution of stellar clusters in the Milky Way might also provide clues about the classification of GC 03. With the distance derived via isochrone fitting and using the transformation matrix shown in Appendix A in Pasetto et al. (2011), we estimate that GC 03 is located at

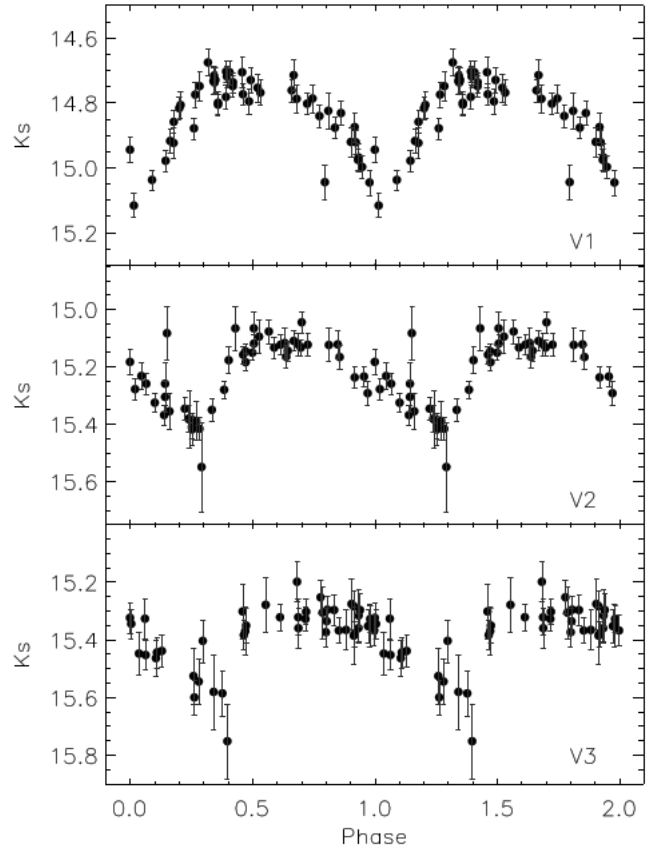


Figure 7. K_s light curves of the RR Lyrae stars found in VVV likely associated with GC 03.

$d_G = 4.2$ kpc from the Galaxy center. OCs older than 6 Gyr are scarce in the Milky Way and all the clusters older than 1 Gyr are located at $d_G > 6$ kpc (Bonatto et al., 2006), although a fraction of clusters might remain undetected in high-extinction areas. Diverse theoretical studies have established that the dissolution time (t_{dis}) for clusters with $M < 10^4 M_\odot$ is lower than a few hundreds of Myr (Lamers et al., 2005), while for OCs with $M \sim 10^4 M_\odot$ it has been estimated a $t_{\text{dis}} \sim 2$ Gyr (Bergond et al., 2001, Gieles et al., 2006). Therefore, it is expected that all the OCs observed nowadays in the inner kpc of the Galaxy are young and massive. Indeed, massive OCs with ages of a few Myr have been found with $R_{\text{GC}} < 4$ kpc (e.g. Figer et al., 2002, Crowther et al., 2006). In this context, GC 03 could only survive as an OC at $R_{\text{GC}} < 4$ kpc if it was as massive as a Galactic GC.

In the case of the Galactic GC population, a significant fraction of the systems lie in the volume defined by $R_{\text{GC}} = 4$ kpc. From the 157 clusters contained in the Harris (2010) catalog, 64 GCs (40%) have $R_{\text{GC}} < 4$ kpc and half of them are found at low Galactic latitudes ($|b| < 5^\circ$). That latter group of GCs has a mean metallicity of $[\text{Fe}/\text{H}] -0.8 \pm 0.4$, which is a similar value to that derived from our spectra for GC 03. Therefore, the position of GC 03 in the Galaxy and its metallicity, similar to that of the bulk of bulge GCs allow us to confirm the globular nature of that cluster.

GC 03 might belong, following the scheme suggested in the classical works by Zinn (1993) and Armandroff (1989), to

³ <http://webda.physics.muni.cz>

the population of disk GCs, rather than to the halo/accreted globulars found in the outer regions of the Galaxy. A prototypical globular included in that metal-rich subgroup and associated with the Milky Way thick disk is 47 Tuc (NGC 104). That GC has a metallicity of $[Fe/H] = -0.7$ with an age of 9.9 Gyr (Carretta et al., 2009, Hansen et al., 2013), which are values similar to those derived in this work. This suggests that GC03 might have been formed together with the disk stellar populations and the metal-rich component of Galactic GCs.

3.7 Radial density profile and spatial distribution

We studied the cluster radial density profile, calculating the stellar density in concentric annuli of width $4''$, centered on the cluster coordinates derived above and using VVV photometry. The results are shown in Figure 8. If the analysis is limited to stars with $K_s < 14.7$ and distances from the center $r < 1.7'$, as done by Froebrich et al. (2007), the radial decay of the stellar density is well represented by a King profile, with $r_c = 0.6 \pm 0.2$ and $r_t = 2.2 \pm 0.7$ as the best-fit core and tidal radii, respectively. These values are slightly larger than those found by Froebrich et al., but comparable within errors, indicating that our VVV stellar counts are consistent with theirs. Nevertheless, when the profile is extended to $r = 7'$, it becomes evident that the background is overestimated by this fit, because the stellar density keeps decreasing beyond $r = 1.7'$. The profile is very flat for $r > 4'$, suggesting that small-scale fluctuations are negligible. However, the tidal radius diverges to huge values if the fit is extended to $r > 2'$. Identical results are found extending the stellar counts down to $K_s < 16.5$. The cause of this unrealistic result is that the density in the range 2–3' is too high than expected for a King profile. The tidal radius can be reduced to 9' excluding the region 2–2.5' from the fit and a minimum value of 4.8 is obtained with the exclusion of the 2–3.5' range. The core radius barely changed in any of these fits and it was always found in the range $r_c = 0.75 \pm 0.05'$. Our results are consistent with those by Kharchenko et al. (2013) where it was also found a very large tidal radius ($8 \pm 2'$), although they do not provide the details of their fit.

Our analysis shows that GC03 is likely more extended than the estimates of Froebrich et al. (2007) reported in the Harris (2010) catalog. However, it is also clear that the cluster density profile is not well represented by a King function. This behavior is typical of a cluster suffering intense tidal stress (see, e.g., Moni Bidin et al., 2011, Carballo-Bello et al., 2012). Indeed, Figure 9 shows the density map generated with stars potentially associated with the GC, with a nearly symmetrical and elongated distribution of stars similar to that observed in GCs with known tidal tails (e.g. Pal 14; see Sollima et al., 2011).

The region with higher density in Figure 9 seems to be contained in an area with radius $r_1 = 0.45$ (inner circle in that plot), while the density of stars beyond $r_2 = 0.95$ (outer circle) is negligible. The distance r_1 is consistent with the core radius derived above for this cluster when only stars with $r < 1.7'$ are considered, while the obtained King tidal radius is much larger than r_2 . At the distance of GC 03, the radius of its observed core is $r_1 = 1.5$ pc and the tentative

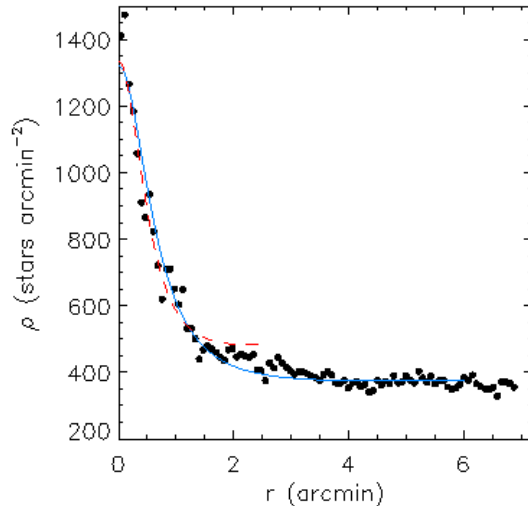


Figure 8. Radial density profile derived for GC03. The red dashed line indicates the best King profile fitted using only those stars with $r < 1.7'$ while the solid blue line corresponds to the fitting including those stars with $r < 7'$.

Table 2. Parameters derived for GC03. Note that proper motions are relative motions (see section 3.2).

Parameter	Result
$[Fe/H]$	-0.9 ± 0.2
d_{\odot} [kpc]	10.8 ± 0.9
d_G [kpc]	4.2 ± 0.1
t [Gyr]	11.3 ± 1.2
v_r [km s^{-1}]	-78 ± 12
$\mu_{\alpha \cos \delta}$ (mas yr^{-1})	-1.3 ± 0.2
μ_{δ} (mas yr^{-1})	1.8 ± 0.3
r_c (arcmin)	0.75 ± 0.05
r_t (arcmin)	>4.8

inner tidal tails expand up to $r_2 = 3.2$ pc from the cluster center.

4 CONCLUSIONS

We have derived fundamental parameters for the stellar cluster 2MASS-GC 03 using MMIRS photometry and spectroscopy and VVV data. Out the 10 stars for which we have obtained spectra, 5 were considered as cluster members based on their proper motions derived from VVV photometry. We have estimated metallicities and radial velocities for field and candidate stars and set mean values for the cluster in $\langle [Fe/H] \rangle = -0.9$ and $\langle v_r \rangle \sim -78 \text{ km s}^{-1}$. With that information, we have established that 2MASS-GC 03 is an intermediate-age system with $t = 11.3$ Gyr at $d_{\odot} = 10.8$ kpc. Its location within the Galaxy and overall properties (summarized in Table 2) confirms its globular nature.

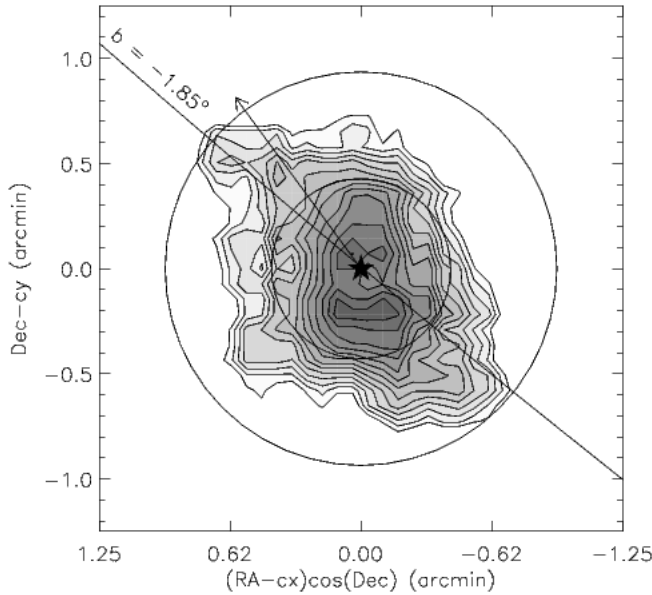


Figure 9. Stellar density contours showing the distribution in the sky of stars belonging to GC 03 according to the decontaminated CMD. The inner and outer circles correspond to the distances $r_1 = 0.45$ arcmin and $r_2 = 0.95$ arcmin respectively. The constant Galactic latitude level at $b = -1.85^\circ$ is overplotted with a solid line while the direction towards the Milky Way center is indicated with an arrow.

ACKNOWLEDGEMENTS

This paper includes data gathered with the 6.5 meter Magellan Telescopes located at Las Campanas Observatory, Chile (program ID: CN2014A-84). JAC-B received support from CONICYT Gemini grant from the Programa de Astronomía del DRI Folio 32130012 and CONICYT-Chile grants FONDECYT Postdoctoral Fellowship 3160502. SRA and CMB were supported by the Fondecyt project number 3140605 and 1150060, respectively. JA-G acknowledges support from the FIC-R Fund, allocated to project 30321072, and from Fondecyt Iniciación 11150916. N.M is supported by CONICYT REDES No. 140042 project. The VVV Survey is supported by ESO, by BASAL Center for Astrophysics and Associated Technologies PFB-06, by FONDAP Center for Astrophysics 15010003, and by the Ministry for the Economy, Development, and Tourism's Programa Inicativa Científica Milenio through grant IC120009, awarded to The Millennium Institute of Astrophysics (MAS). Partially based on data products from observations made with ESO Telescopes at the La Silla or Paranal Observatories under ESO programme ID 179.B-2002. This publication makes use of data products from the Two Micron All Sky Survey, which is a joint project of the University of Massachusetts and the Infrared Processing and Analysis Center/California Institute of Technology, funded by the National Aeronautics and Space Administration and the National Science Foundation. Thanks to K. Peña-Ramírez and J. M. Corral-Santana for their help during the spectra reduction.

REFERENCES

- Armandroff T. E., 1989, *AJ*, 97, 375
 Ashman K. M., Zepf S. E., 1992, *ApJ*, 384, 50
 Balbinot E., Santiago B. X., da Costa L., Maia M. A. G., Majewski S. R., Nidever D., Rocha-Pinto H. J., Thomas D., Wechsler R. H., Yanny B., 2013, *ApJ*, 767, 101
 Bergond G., Leon S., Guibert J., 2001, *A&A*, 377, 462
 Bonatto C., Bica E., 2007, *MNRAS*, 377, 1301
 Bonatto C., Bica E., 2010, *A&A*, 516, A81
 Bonatto C., Bica E., 2011, *MNRAS*, 415, 313
 Bonatto C., Kerber L. O., Bica E., Santiago B. X., 2006, *A&A*, 446, 121
 Borissova et al. 2011, *A&A*, 532, A131
 Borissova et al. 2014, *A&A*, 569, A24
 Bressan A., Marigo P., Girardi L., Salasnich B., Dal Cero C., Rubele S., Nanni A., 2012, *MNRAS*, 427, 127
 Brogaard K., VandenBerg D. A., Bruntt H., Grundahl F., Frandsen S., Bedin L. R., Milone A. P., Dotter A., Feiden G. A., Stetson P. B., Sandquist E., Miglio A., Stello D., Jessen-Hansen J., 2012, *A&A*, 543, A106
 Buckner A. S. M., Froebrich D., 2014, *MNRAS*, 444, 290
 Cabrera-Lavers A., González-Fernández C., Garzón F., Hammersley P. L., López-Corredoira M., 2008, *A&A*, 491, 781
 Carballo-Bello J. A., Gieles M., Sollima A., Koposov S., Martínez-Delgado D., Peñarrubia J., 2012, *MNRAS*, 419, 14
 Carraro G., 2005, *ApJL*, 621, L61
 Carretta E., Bragaglia A., Gratton R. G., Lucatello S., Catanzaro G., Leone F., Bellazzini M., Claudi R., D'Orazi V., Momany Y., Ortolani S., Pancino E., Piotto G., Rieco-Blanco A., Sabbi E., 2009, *A&A*, 505, 117
 Crowther P. A., Hadfield L. J., Clark J. S., Negueruela I., Vacca W. D., 2006, *MNRAS*, 372, 1407
 Davies B., Bastian N., Gieles M., Seth A. C., Mengel S., Konstantopoulos I. S., 2011, *MNRAS*, 411, 1386
 Figier D. F., Najarro F., Gilmore D., Morris M., Kim S. S., Serabyn E., McLean I. S., Gilbert A. M., Graham J. R., Larkin J. E., Levenson N. A., Teplitz H. I., 2002, *ApJ*, 581, 258
 Froebrich D., Meusinger H., Scholz A., 2007, *MNRAS*, 377, L54
 Froebrich D., Scholz A., Raftery C. L., 2007, *MNRAS*, 374, 399
 Frogel J. A., Stephens A., Ramírez S., DePoy D. L., 2001, *AJ*, 122, 1896
 Gieles M., Portegies Zwart S. F., Baumgardt H., Athanassoula E., Lamers H. J. G. L. M., Sipior M., Leenaarts J., 2006, *MNRAS*, 371, 793
 González-Fernández C., Asensio Ramos A., Garzón F., Cabrera-Lavers A., Hammersley P. L., 2014, *ApJ*, 782, 86
 Hansen B. M. S., Kalirai J. S., Anderson J., Dotter A., Richer H. B., Rich R. M., Shara M. M., Fahlman G. G., Hurley J. R., King I. R., Reitzel D., Stetson P. B., 2013, *Nat.*, 500, 51
 Harris W. E., 2010, ArXiv:1012.3224
 Huijse P., Estevez P. A., Zegers P., Principe J. C., Protopapas P., 2011, *IEEE Signal Processing Letters*, 18, 371
 Janes K. A., Phelps R. L., 1994, *AJ*, 108, 1773
 Joshi Y. C., 2005, *MNRAS*, 362, 1259

- Jurić et al. 2008, *ApJ*, 673, 864
 Kausch et al. 2015, *A&A*, 576, A78
 Kharchenko N. V., Piskunov A. E., Schilbach E., Röser S., Scholz R.-D., 2013, *A&A*, 558, A53
 Kim D., Jerjen H., Milone A. P., Mackey D., Da Costa G. S., 2015, *ApJ*, 803, 63
 Kobulnicky et al. 2005, *AJ*, 129, 239
 Koposov S., de Jong J. T. A., Belokurov V., Rix H.-W., Zucker D. B., Evans N. W., Gilmore G., Irwin M. J., Bell E. F., 2007, *ApJ*, 669, 337
 Krusberg Z. A. C., Chaboyer B., 2006, *AJ*, 131, 1565
 Laevens et al. 2014, *ApJL*, 786, L3
 Lamers H. J. G. L. M., Gieles M., Bastian N., Baumgardt H., Kharchenko N. V., Portegies Zwart S., 2005, *A&A*, 441, 117
 Longmore A. J., Kurtev R., Lucas P. W., Froebrich D., de Grijs R., Ivanov V. D., Maccarone T. J., Borissova J., Ker L. M., 2011, *MNRAS*, 416, 465
 Mauro F., Moni Bidin C., Chené A.-N., Geisler D., Alonso-García J., Borissova J., Carraro G., 2013, *RMXAA*, 49, 189
 McLeod B., Fabricant D., Nystrom G., McCracken K., Amato S., Bergner H., Brown W., Burke M., Chilingarian I., Conroy M., Curley D., Furesz G., Geary J., Hertz E., Holwell J., Matthews A., Norton T., Park S., et al. 2012, *PASP*, 124, 1318
 McWilliam A., Zoccali M., 2010, *ApJ*, 724, 1491
 Minniti D., Lucas P. W., Emerson J. P., Saito R. K., Hempel M., Pietrukowicz P., Ahumada A. V., et al. 2010, *New Astronomy*, 15, 433
 Minniti et al. 2011, *A&A*, 527, A81
 Moni Bidin et al. 2011, *A&A*, 535, A33
 Muñoz R. R., Geha M., Côté P., Vargas L. C., Santana F. A., Stetson P., Simon J. D., Djorgovski S. G., 2012, *ApJL*, 753, L15
 Muraveva T., Palmer M., Clementini G., Luri X., Cioni M.-R. L., Moretti M. I., Marconi M., Ripepi V., Rubele S., 2015, *ApJ*, 807, 127
 Nataf D. M., Gould A. P., Pinsoneault M. H., Udalski A., 2013, *ApJ*, 766, 77
 Pasetto S., Grebel E. K., Berczik P., Chiosi C., Spurzem R., 2011, *A&A*, 525, A99
 Roeser S., Demleitner M., Schilbach E., 2010, *AJ*, 139, 2440
 Saito et al. 2012, *A&A*, 537, A107
 Simpson J. P., Cotera A. S., 2004, in American Astronomical Society Meeting Abstracts #204 Vol. 36 of Bulletin of the American Astronomical Society, Massive Star Clusters in the ASCA Galactic Plane Survey. p. 734
 Skrutskie et al. 2006, *AJ*, 131, 1163
 Smette et al. 2015, *A&A*, 576, A77
 Smith L. C., 2015, PhD thesis, University of Hertfordshire
 Solin O., Haikala L., Ukkonen E., 2014, *A&A*, 562, A115
 Sollima A., Valls-Gabaud D., Martinez-Delgado D., Fliri J., Peñarrubia J., Hoekstra H., 2011, *ApJL*, 730, L6+
 Stetson P. B., 1987, *PASP*, 99, 191
 Valenti E., Ferraro F. R., Origlia L., 2007, *AJ*, 133, 1287
 Willman B., Blanton M. R., West A. A., Dalcanton J. J., Hogg D. W., Schneider D. P., Wherry N., Yanny B., Brinkmann J., 2005, *AJ*, 129, 2692
 York et al. 2000, *AJ*, 120, 1579
 Zinn R., 1985, *ApJ*, 293, 424
 Zinn R., 1993, in G. H. Smith & J. P. Brodie ed., The

Globular Cluster-Galaxy Connection Vol. 48 of Astronomical Society of the Pacific Conference Series, The Galactic Halo Cluster Systems: Evidence for Accretion. pp 38–+

Table 3. Parameters derived for the RR Lyrae found in GC 03.

ID	RA [J2000]	Dec [J2000]	$\langle Ks \rangle$	Ampl.	P (d)	d_{\odot} (kpc)
V1	253.0405607	-47.077880	14.88	0.45	0.84310	11.2
V2	253.0267025	-47.717799	15.21	0.50	0.54171	10.5
V3	252.8666458	-46.995242	15.36	0.55	0.55330	10.8